JOURNAL OF PROPULSION AND POWER
Vol. 18, No. 1, January–February 2002

Selection of Actuators and Sensors for Surge Control

Marc van de Wal,* Frank Willems,† and Bram de Jager‡
Eindhoven University of Technology, 5600 MB Eindhoven, The Netherlands

For surge control in compression systems, a suitable combination of actuators and sensors must be selected. The goal is to identify the combinations for which there exists a controller that locally stabilizes the linearized compression system model and meets additional control objectives. The latter are quantified in terms of a bound on an $\mathcal{H}_\infty$ norm. With this we aim to stay close to the nominal operating point in the face of disturbances, noise, and actuator limitations. The considered selection method is more rigorous than previously found in literature, in the sense that multivariable, dynamic output feedback is the focus and that different performance specifications are handled simultaneously. Though the method was originally developed for linear systems, it can be used for the nonlinear compression system model by linearizing the model on a grid of nominal operating points. Among the proposed actuators and sensors, the close-coupled valve and mass flow sensor are identified as the most promising. The results are sustained by the physics of the problem.

Nomenclature

F	=	parameter in approximation of Ψ_c
G	=	generalized plant
$\bar{G}_{\mathrm{nl}}/\bar{G}$	=	nonlinear/linear nominal plant model
H	=	parameter in approximation of Ψ_c
K	=	controller
K_T	=	throttle area parameter
M	=	generalized closed-loop system
$\dot{m}_c$	=	compressor mass flow
$\tilde{t}/t$	=	dimensionless/dimensional time
$\tilde{t}_e$	=	dimensionless end time of simulation
u	=	manipulated variables (inputs)
u_1/u_2	=	dimensionless close-coupled/bleed valve parameter
u_3	=	dimensionless movable wall velocity
$u_{3_{\max,1}}$	=	dimensionless maximum velocity of movable wall
$u_{3_{\max,2}}$	=	dimensionless maximum displacement of movable wall
V	=	shaping filter
W	=	weighting filter
$\bar{w}/w$	=	unscaled/scaled exogenous variables
$w_1/w_2/w_3$	=	dimensionless inlet pressure/outlet flow/compressor pressure disturbance
$w_{4,\ldots,7}$	=	dimensionless sensor noise
x_1	=	dimensionless compressor mass flow
x_2	=	dimensionless plenum pressure rise
y	=	measured variables (outputs)
y_1	=	dimensionless compressor mass flow
y_2	=	dimensionless plenum pressure rise
y_3/y_4	=	dimensionless total/static compressor face pressure
$\bar{z}/z$	=	unscaled/scaled controlled variables
z_1	=	dimensionless compressor mass flow
z_2	=	dimensionless plenum pressure rise
$z_{3,4,5}$	=	dimensionless manipulated variables
α/α_{cc}	=	stable mass flow indicator without/with close-coupled valve
γ	=	desired nominal performance level
Δp	=	plenum pressure rise
$\Delta\tilde{t}$	=	dimensionless time between disturbances
θ_1/θ_2	=	magnitude of noise on mass flow/pressure measurement
λ_1/λ_2	=	eigenvalue with largest/smallest absolute-valued real part
$\rho_{1,\ldots,4,5_1,5_2}$	=	design parameters in W
$\bar{\sigma}(\cdot)$	=	maximum singular value of a matrix
$\upsilon_{1,2,3}$	=	steady-state gain of $V_{1,2,3}$
Φ_T	=	throttle characteristic or load line
Ψ_c	=	compressor characteristic or speed line
Ψ_{c0}	=	parameter in approximation of Ψ_c
$\tilde{\omega}/\omega$	=	dimensionless/dimensional angular frequency
$\tilde{\omega}_{0,\ldots,5}$	=	break frequencies in design filters

Subscripts

i	=	ith (diagonal) entry
$\|T\|_\infty$	=	$\mathcal{H}_\infty$ norm of transfer function matrix T
0	=	nominal value

Received 26 June 1998; revision received 1 May 2001; accepted for publication 13 August 2001.

*Control Engineer, Department of Mechanical Engineering; currently Control Engineer, Philips CFT, Mechatronics Research, P.O. Box 218/SAQ-2116, 5600 MD Eindhoven, The Netherlands; M.M.J.van.de.Wal@philips.com.

†Research Scientist Powertrains, Department of Mechanical Engineering; currently Research Scientist Powertrains, TNO Automotive, Building EF 0-31, P.O. Box 6033, 2600 JA Delft, The Netherlands; Willems@wt.tno.nl.

‡Universitair Docent, Department of Mechanical Engineering, P.O. Box 513; A.G.de.Jager@wfw.wtb.tue.nl.

I. Introduction

COMPRESSORS are widely used, e.g., to compress air in jet engines. Toward small mass flow, the operating envelope of compressors is hampered by rotating stall and surge. Surge is characterized by large-amplitude fluctuations of pressure and mass flow and results in a limit-cycle oscillation. The aerodynamic flow instabilities can lead to hazardous conditions because of large mechanical and thermal loads and loss of thrust. From efficiency and, especially, safety points of view, it is desirable to enlarge the region in which stable compressor operation is possible. Among the various ways to achieve this, active control is a recent and promising option. Surveys of rotating stall and surge control can be found in Refs. 1–3. This paper will focus on suppression of surge in the face of disturbances, actuator limitations, and noisy measurements.

To act on a system (plant) and to acquire information on the system's behavior, suitable variables manipulated by the controller (plant inputs or actuators) and suitable variables supplied to the controller (plant outputs or sensors) have to be selected. This process is called input/output (IO) selection. A particular combination of inputs and outputs is called an IO set. IO selection amounts to selecting an appropriate number, place, and type of actuators and

sensors. Sensible IO selection is crucial because the IO set affects the achievable performance and expenses of hardware, implementation, operation, and maintenance. A review of IO selection methods, also related to flight propulsion, is given in Ref. 4. Here, the IO selection method proposed in Ref. 5 is employed. It identifies the IO set(s) for which there exists a stabilizing controller achieving $\mathcal{H}_\infty$ performance specifications. For the considered compression system of a Garrett GT45 turbocharger, three candidate actuators and four sensors are proposed, which are also among those examined in Ref. 6. All results in the present paper are based on a model of the compression system.

The main contribution of this paper is to perform IO selection for the surge control problem more rigorously than previously done in the literature: 1) selection of both inputs and outputs among various candidates is addressed; 2) performance can be handled in a general way, e.g., by simultaneously considering disturbances, sensor noise, and limitations on mass flow, pressure, and control inputs; 3) the controller is of the dynamic output feedback type, for which the performance requirments can be more easily met than for a more restrictive controller type. In Ref. 7 only 1) placement of an air bleeding actuator is considered, based on 2) minimizing the bleed flow, using 3) a static state feedback controller. In Ref. 6 only 1) 1×1 IO sets are examined based on 2) their ability to increase the operating range for which stabilization can be achieved, using 3) a static output feedback controller. To some extent, the effect of limited bandwidth and gain constraints on the ability to stabilize the system is also investigated in Ref. 6, as well as the prospects for static state feedback with single actuators under disturbances. In Refs. 6 and 7 and here the nonlinearity of the compression system is only indirectly dealt with by considering linearizations in various nominal operating points. The IO selection method from Ref. 5 is developed for linear systems and $\mathcal{H}_\infty$ performance specifications, but it is shown that it can cope quite well with nonlinear systems and more general performance specifications. It is also investigated which candidate inputs and outputs are preferred under different operating conditions, and the results are given a physical interpretation. The IO selection results help to decide on the actuators and sensors to be used for an experimental gas turbine rig in the Energy Technology Laboratory of Eindhoven University of Technology, the Netherlands. Various concepts for active surge control are experimentally verified with this rig, but this will be reported elsewhere.

This paper is organized as follows. In Sec. II the basic ideas of the IO selection method are summarized. Section III then sketches the control problem and proposes the candidate actuators and sensors, whereas Sec. IV quantifies the control objectives. In Sec. V, optimal controllers are designed to obtain insight into the importance of each actuator and sensor. Section VI provides the IO selection results and shows simulations for two promising IO sets. Finally, Sec. VII draws the main conclusions. For more details on the IO selection method and the application to the compression system, see Refs. 8 and 9.

II. IO Selection Method

The model of the compression system to be considered is nonlinear, but the IO selection method from Ref. 5 is essentially developed for linear systems. Therefore, the IO selection method will first be explained for linear systems, and later it will be discussed how it can be used for nonlinear systems.

Consider a finite-dimensional, linear, and time-invariant control system in the setup of Fig. 1. Four sets of variables play a role: the measured variables (outputs) y, the manipulated variables (inputs) u, the exogenous variables w (like references, disturbances, and noise), and the controlled variables z that should be small (like regulation and tracking errors). Suitable u and y are to be determined by IO selection. The notation $\{\bar{\cdot}\}$ distinguishes the physical exogenous and controlled variables related to $\bar{G}$ from the design variables related to G. The setup in Fig. 1 does not explicitly account for model uncertainties because nominal performance (NP) is the focus here.

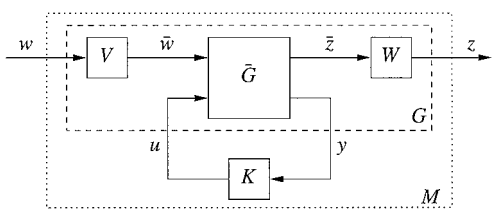

Fig. 1 Control system setup.

Many NP problems can be formulated qualitatively as keeping the controlled variables $\bar{z}$ acceptably small for a class of exogenous variables $\bar{w}$. Assume that such a problem can be quantified as keeping a particular norm ("amplification measure") of the closed-loop system smaller than a desired value. The $\mathcal{H}_\infty$ norm is the focus here. This norm naturally arises when shaping the magnitude of certain closed-loop transfer functions, when minimizing the worst-case response/energy/power of $\bar{z}$ for sinusoidal/energy-bounded/power-bounded $\bar{w}$, or when uncertainties have to be characterized. For a stable system $T(s)$ the $\mathcal{H}_\infty$ norm is defined as

$$\|T(s)\|_\infty := \sup_\omega \bar{\sigma}[T(j\omega)] \tag{1}$$

A meaningful control problem formulation accounts for the (relative) magnitudes of the exogenous variables in $\bar{w}$, the (relative) importance of the controlled variables in $\bar{z}$, and the frequency dependence of $\bar{w}$ and $\bar{z}$. For this purpose diagonal transfer function matrices (TFM) V and W are introduced. The shaping filter V characterizes the (expected or known) energy or power distribution in the frequency domain of the components in $\bar{w}$. The weighting filter W indicates which frequencies are crucial to be suppressed for the components in $\bar{z}$. Typically, $|V_i|$ is large for frequencies where $|\bar{w}_i|$ is large, whereas $|W_i|$ is large for frequencies where $|\bar{z}_i|$ must be small.

For given V and W the aim of suboptimal controller design is to find a stabilizing K that achieves an $\mathcal{H}_\infty$ norm bound γ on the weighted closed-loop system: $\|M\|_\infty < \gamma$, with $\gamma > 0$ the desired NP level (typically, $\gamma = 1$). The aim of optimal controller design is to find a stabilizing K that minimizes $\|M\|_\infty$ ($\mathcal{H}_\infty$ optimization). The IO selection method adopts the suboptimal approach for two reasons. First, achieving the smallest $\|M\|_\infty$ over all IO sets would imply using (almost) all candidate inputs and outputs. Second, checking $\|M\|_\infty < \gamma$ for a single IO set requires less computation time than computing the minimum $\|M\|_\infty$, which makes the IO selection more efficient.

IO selection is based on checking a set of conditions for the existence of a stabilizing K achieving $\|M\|_\infty < \gamma$. IO sets passing all conditions are called *viable*, the others *nonviable*. These conditions involve two algebraic Riccati equations that arise in the parameterization of all such controllers.[10] The IO selection conditions (or controller existence conditions) are only given an interpretation here. For mathematical details see Ref. 11 (Chapters 16 and 17) and Ref. 9, (Chapter 4). Essentially, IO selection involves the following checks:

1) Check if G is stabilizable (the unstable modes are controllable) by u and detectable (the unstable modes are observable) by y. This is necessary and sufficient for the existence of a stabilizing controller with no additional requirement on $\|M\|_\infty$. Note that V and W must be stable because their modes are uncontrollable by u and unobservable by y.

2) Check if the open-loop direct feedthrough from w to z is not too large because K can only affect a certain part of it.

3) Check if a controller K with full information on w and the states of G can meet $\|M\|_\infty < \gamma$. This can be seen as the situation with the perfect output set.

4) Check if a controller K with full access to z and the states of G can meet $\|M\|_\infty < \gamma$. This can be seen as the situation with the perfect input set.

5) Based on the results from checks 3 and 4, check if the combination of imperfect input and output set can meet $\|M\|_\infty < \gamma$. This is a kind of coupling condition to check if a suitable combination of state estimation and state estimate feedback can meet $\|M\|_\infty < \gamma$.

The conditions are checked in succession. As soon as one condition fails, the other conditions are not checked. With this procedure a large number of IO sets can be assessed because the time-consuming process of complete controller design for each IO set is avoided.

To further improve efficiency, IO selection is split into three steps: 1) input selection using the full output set, 2) output selection using the full input set, and 3) combined input/output selection for the IO sets made up of the candidates passing steps 1 and 2, except the full input and output set. This approach can significantly reduce the total number of candidates to be checked.

For nonlinear systems an equivalent of the linear $\mathcal{H}_\infty$ control problem can be formulated. This nonlinear $\mathcal{H}_\infty$ control problem is locally solvable in a region around an equilibrium if the $\mathcal{H}_\infty$ problem for the corresponding linearization is solvable (Ref. 12, Chapter 7). Solvability of the linear $\mathcal{H}_\infty$ problem is thus sufficient for local solvability of the nonlinear $\mathcal{H}_\infty$ problem. In practice (as for the compression system), one is often interested in a range of equilibria (or nominal operating points) rather than in one particular equilibrium. The IO selection conditions can then be applied to multiple linearizations for a grid of operating points. IO sets that are accepted for the first operating point are passed to the next operating point, until the complete grid has been handled. The ultimately accepted IO sets may not be viable for other points than those in the grid because the (unknown) local regions of attraction may not link up or overlap. To investigate global viability, the attraction regions could be computed, or, less rigorously, closed-loop simulations could be performed. If the grid is denser, the chance of incorrectly accepting IO sets will in general decrease, but the computation time might increase.

III. Compressor Control Problem

A model of a high-speed, single-stage, radial compressor in a turbocharger is considered. This turbocharger (Garrett GT45) is part of a gas turbine installation (see Ref. 13). The model is schematized in Fig. 2, and the main parameters are listed in Table 1. In the employed Greitzer lumped parameter model,[14] the compressor is replaced by an actuator disk, i.e., a plane accounting for the pressure rise. The compressor duct is represented by a constant-area pipe that accounts for the fluid dynamics. The flow in this duct is assumed to be one-dimensional and incompressible. The pressurized fluid is discharged into a large plenum. Finally, the fluid is delivered to a process requiring a certain pressure and/or mass flow, represented by a throttle in the exit duct across which the pressure drops. The inertia effects in this relatively short duct are neglected.

Table 1 Main parameters in the compression system model

Symbol	Value (range)	Meaning
	Speed-independent parameters	
a	340 m/s	Speed of sound
A_c	5.38×10^{-3} m^2	Compressor flow-through area
A_p	1.13 m^2	Plenum movable wall area
c_1	7.65×10^{-1}	Close-coupled valve capacity parameter
c_2	4.84×10^{-1}	Bleed valve capacity parameter
L_c	1.00 m	Equivalent compressor duct length
N_b	6	Number of rotor blades
p_a	1.01×10^5 Pa	Absolute ambient air pressure
r_T	7.50×10^{-2} m	Rotor-tip radius
V_p	2.66 m^3	Plenum volume
ρ_a	1.20 kg/m^3	Ambient air density
ω_H	15.29 rad/s	Helmholtz frequency
	Speed-dependent parameters	
B	[10.27, . . . , 25.68]	Compressor stability parameter
M_T	[0.92, . . . , 2.31]	Rotor-tip Mach number
ω_c	$(2\pi/60)$ [40×10^3, . . . , 100×10^3] rad/s	Compressor rotational speed

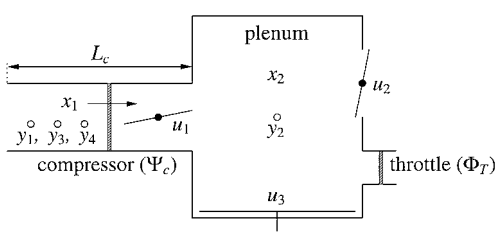

Fig. 2 Compression system with candidate actuators u and sensors y.

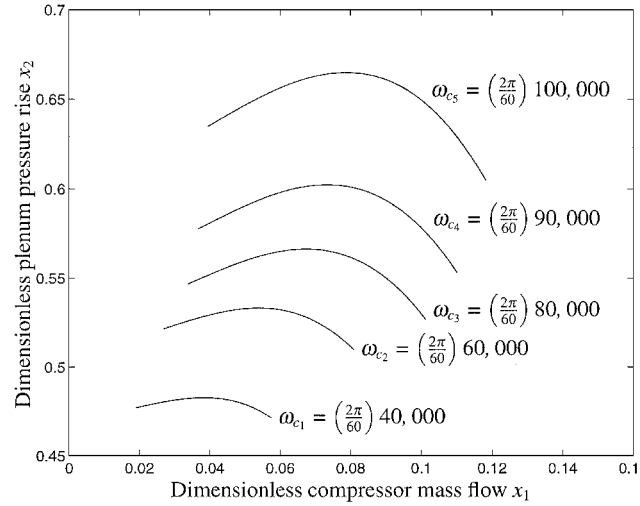

Fig. 3 Compressor map with $\Psi_c[x_1(\omega_c), \omega_c]$ for various rotor speeds ω_c [rad/s].

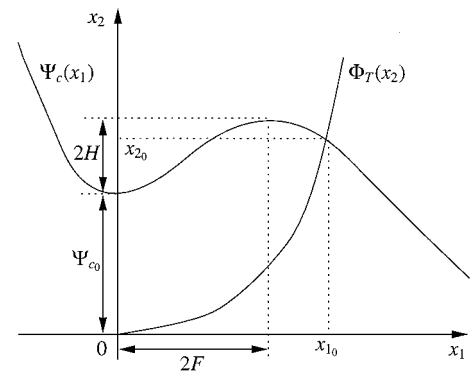

Fig. 4 Impression of the compressor characteristic (6) and throttle characteristic (7).

The state of a compression system is in general determined by four dimensionless variables: the compressor mass flow, the plenum pressure rise, the rotor speed, and the temperature (or a related variable, like the efficiency). The last variable is usually not needed to characterize the surge region. The compressor mass flow and plenum pressure rise are made dimensionless as follows:

$$x_1(\omega_c) = \frac{\dot{m}_c}{\omega_c r_T \rho_a A_c}, \qquad x_2(\omega_c) = \frac{\Delta p}{\omega_c^2 r_T^2 \rho_a / 2} \tag{2}$$

In steady-state $x_1(\omega_c)$, $x_2(\omega_c)$, and ω_c are connected via the compressor characteristic or speed line $\Psi_c[x_1(\omega_c), \omega_c]$, as shown in Fig. 3. So, in steady state only two of $x_1(\omega_c)$, $x_2(\omega_c)$, and ω_c are independent.

The original Greitzer model is restricted to constant speeds ω_c. Based on conservation of mass and momentum, on the preceding assumptions, and on the assumption, that the (quasi-steady) speed line is also valid during transients, this model provides two differential equations in $x_1(\omega_c)$ and $x_2(\omega_c)$ for a given constant speed ω_c:

$$\dot{x}_1(\omega_c) = B(\omega_c)\{\Psi_c[x_1(\omega_c), \omega_c] - x_2(\omega_c)\} \tag{3}$$

$$\dot{x}_2(\omega_c) = [1/B(\omega_c)]\{x_1(\omega_c) - \Phi_T[x_2(\omega_c)]\} \tag{4}$$

with

$$B(\omega_c) = (\omega_c r_T/2a)\sqrt{V_p/A_c L_c} \tag{5}$$

In the sequel the dependence on ω_c is skipped from the notation because only one speed at a time will be considered. This is also the reason why a model including the speed dynamics[15] is not used. The five speeds in Fig. 3 are used. For fixed ω_c the compressor

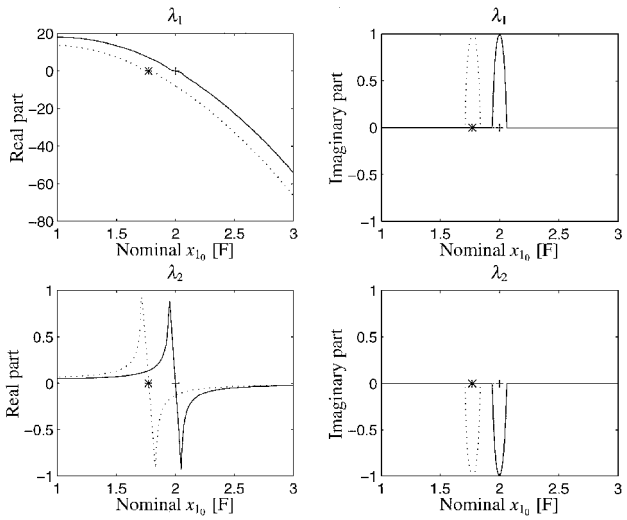

Fig. 5 Eigenvalues of the linearization $\bar{G}$ for rotor speed $\omega_{c_3} = (2\pi/60)80{,}000$ [rad/s], without u_1 (——) and with u_1(· · · ·). λ_1 and λ_2 are the eigenvalues with the largest and smallest absolute-valued real parts, respectively. The linearized system excluding u_1 is stable for $x_{1_0} > \alpha F$ (+), and the linearized system including u_1 is stable for $x_{1_0} > \alpha_{cc} F$(∗).

characteristics is approximated by a third-order polynomial in x_1 (see Fig. 4):

$$\Psi_c(x_1) = \Psi_{c0} + H\left[1 + \tfrac{3}{2}(x_1/F - 1) - \tfrac{1}{2}(x_1/F - 1)^3\right] \qquad (6)$$

The parameters Ψ_{c_0}, H, and F depend on ω_c, and they are determined from data for the experimental rig (Ref. 9, Appendix C). For $x_2 \geq 0$ the throttle characteristic is modeled as (see Fig. 4):

$$\Phi_T(x_2) = K_T\sqrt{x_2} \qquad (7)$$

The downstream process requirements determine K_T. Here K_T is set such that the intersection of Ψ_c and Φ_T yields the desired operating point (x_{1_0}, x_{2_0}), see Fig. 4. For each speed the investigated range for x_{1_0} is given by $[F, 3F]$, with $x_{1_0} = 2F$ the value where $\Psi_c(x_1)$ peaks and where the efficiency is usually highest.[1] Mass flows outside this range are assumed to be of less practical relevance here. Emphasis will be on $\Psi_c(x_1)$ corresponding to $\omega_{c_3} = (2\pi/60)80{,}000$ [rad/s], which is close to the highest speed for which reliable experimental data are available, also in the surge area. Based on the conclusions in Ref. 6, it is expected that the control goal (formulated below) is more difficult to achieve at high speeds. This will be verified in Secs. V.A and VI.

The stability of an equilibrium (x_{1_0}, x_{2_0}) can be investigated by linearizing Eqs. (3) and (4). The two eigenvalues (λ_1 and λ_2, see Fig. 5) have negative real parts, if and only if

$$\left.\frac{\partial\Psi_c(x_1)}{\partial x_1}\right|_{x_{1_0}} < \left.\left(\frac{\partial\Phi_T(x_2)}{\partial x_2}\right)^{-1}\right|_{x_{2_0}}$$

$$\left.\frac{\partial\Psi_c(x_1)}{\partial x_1}\right|_{x_{1_0}} < \left.\frac{1}{B^2}\frac{\partial\Phi_T(x_2)}{\partial x_2}\right|_{x_{2_0}} \qquad (8)$$

For $x_{1_0} \in [F, 3F]$ the left inequality is always fulfilled, but the right one is not. The part of $[F, 3F]$ corresponding to unstable (stable) linearizations is called the "unstable (stable) mass flow range" denoted by $[F, \alpha F]$ $[(\alpha F, 3F)]$. Parameter α, $1 \leq \alpha < 2$, decreases for decreasing B parameters [Eq. (5)]. Compared to the values of B between 0.27 and 2.7 found in literature (Ref. 16, Sec. 3.1), the system considered here has much larger values ranging from 10 (for ω_{c_1}) to 26 (for ω_{c_5}). As Fig. 5 shows, the linearizations are unstable on almost the entire positively sloped part of Ψ_c, because $1.9996 \leq \alpha < 2$.

The NP control goal is to guarantee stable compressor operation under exogenous disturbances and actuator limitations, locally around nominal operating points (x_{1_0}, x_{2_0}). This is particularly important for unstable linearizations. To make it possible to impose that the state trajectory should remain close to (x_{1_0}, x_{2_0}), $\bar{z}_1$ and $\bar{z}_2$ represent the deviations of x_1 and x_2 from x_{1_0} and x_{2_0}. The inputs u to be proposed are limited and also included in $\bar{z}$. The following disturbances are considered: inlet pressure disturbances $\bar{w}_1$ (caused by disturbances in upstream processes, e.g., due to aircleaner effects), outlet flow disturbance $\bar{w}_2$ (caused by downstream processes, e.g., due to pressure pulsations caused by a combustion chamber), compressor pressure disturbance $\bar{w}_3$ (e.g., caused by local unsteady flow in the rotor or diffuser). Finally, $\bar{w}$ includes sensor noise corresponding to the outputs y to be proposed.

To manipulate and measure system behavior, the control system should include actuators and sensors. With one properly chosen actuator and sensor the first IO selection condition can be fulfilled (Ref. 8, Sec. 3.4), i.e., for all nominal operating points local stabilization can be guaranteed with a 1×1 IO set. In practice, however, stabilization must be achieved in the face of disturbances, noise, and actuator limitations, and this may not be possible with a 1×1 IO set. The candidate actuators and sensors in Fig. 2 are also among those examined in Ref. 6.

The three (dimensionless) candidate inputs are close-coupled valve parameter u_1, bleed valve parameter u_2, and movable wall velocity u_3. Fast valves are considered. Input u_2 could be interpreted as the available flow-through area while u_1, owing to an input transformation (Ref. 9, Appendix C) to obtain the input affine model in Eq. (9), is proportional to pressure loss. The nominal values $u_{1_0} \in [1, \infty)$ and $u_{2_0} \in [0, 1]$ are chosen such that the pressure drop across the valves can be larger or smaller than nominal, while the efficiency loss is acceptable: $u_{1_0} = 1.72$ is such that the pressure drop across the close-coupled valve is 1% of the maximum pressure rise $\Psi_c(2F)$ for a fully open valve, i.e., for $u_{1_0} = 1$; $u_{2_0} = 1.85 \times 10^{-3}$ is such that the mass flow through the bleed valve is 1% of $2F$ (for $u_{2_0} = 0$, the bleed valve is fully closed). Both valves are rather large. It is difficult to compare the relative merits of actuators with 1% pressure or 1% bleed loss in steady state. By increasing the losses, the actuator constraints become less tight, and the system might be easier to control. The movable wall has negligible steady-state losses and is better in this respect. One way to achieve zero steady-state losses with a close-coupled valve or a bleed valve is to use one-sided control. This is demonstrated for a bleed valve in Ref. 17.

With the close-coupled valve $[F, \alpha_{cc} F]$ denotes the unstable mass flow range, and $(\alpha_{cc} F, 3F]$ denotes the stable mass flow range. This valve modifies the shape of Ψ_c, resulting in an enlarged open-loop stable operating range (see Fig. 5). So, α_{cc} is smaller than α without u_1: for the five speeds $1.7448 \leq \alpha_{cc} \leq 1.7974$. The stable mass flow range increases to the left (α_{cc} decreases) for increasing u_{1_0}. The movable wall's nominal velocity u_{3_0} is zero.

The four (dimensionless) candidate outputs are compressor mass flow $y_1 = x_1$, plenum pressure rise $y_2 = x_2$, total compressor face pressure y_3, and static compressor face pressure y_4.

For $x_2 \geq 0$ the nonlinear compression system model including all relevant variables is now given by (for details, see Ref. 9, Appendix C)

$$\bar{G}_{\text{nl}}: \begin{cases} \dot{x}_1 = B\left[\Psi_c(x_1) - x_2 + \bar{w}_1 + \bar{w}_3 - \left(\dfrac{x_1|x_1|}{c_1}\right)u_1\right] \\ \dot{x}_2 = \dfrac{1}{B}[x_1 - \Phi_T(x_2) + \bar{w}_2 - c_2\sqrt{x_2}u_2] - \left(\dfrac{\rho_a a^2}{p_a}x_2 + \dfrac{2}{M_T^2}\right)u_3 \\ \bar{z}_i = x_i - x_{i_0}, \qquad i = 1, 2 \\ \bar{z}_{j+2} = u_j - u_{j_0}, \qquad j = 1, 2, 3 \\ y_1 = x_1 + \bar{w}_4 \\ y_2 = x_2 + \bar{w}_5 \\ y_3 = x_2 - \Psi_c(x_1) - \bar{w}_1 - \bar{w}_3 + \bar{w}_6 + \left(\dfrac{x_1|x_1|}{c_1}\right)u_1 \\ y_4 = -x_1^2 + x_2 - \Psi_c(x_1) - \bar{w}_1 - \bar{w}_3 + \bar{w}_7 + \left(\dfrac{x_1|x_1|}{c_1}\right)u_1 \end{cases} \qquad (9)$$

In the remainder the main focus is on linearizations of this model. Unless explicitly noted, x, $\bar{w}$, w, $\bar{z}$, z, u, and y are used to represent the corresponding variables of the linearization.

IV. $\mathcal{H}_\infty$ Performance Specifications

The control objectives are quantified via the design filters V and W (Sec. IV.A). Some design parameters are determined by simulations of the nonlinear plant that is controlled by linear controllers using the full IO set (Sec. IV.B).

A. Design Filters

The computational effort for checking an IO set is affected by the order of G. To limit this effort, the diagonal entries in V and W are restricted to low-order transfer functions. This is justified if the control objectives can be represented accurately enough, as assumed here. The Helmholtz frequency is

$$\omega_H = a\sqrt{A_c/V_pL_c} \tag{10}$$

It is the natural frequency of the oscillations of the gas in the compressor duct and the plenum in the absence of the compressor and throttle. It is used for time scaling: $\tilde{t} = t\omega_H$. In the frequency domain the dimensionless frequency $\tilde{\omega} = \omega/\omega_H$ comes into play, with ω in radians per second.

The shaping filters for $\bar{w}_1$, $\bar{w}_2$, and $\bar{w}_3$ are specified as follows:

$$V_i(s) = \upsilon_i/(s/\tilde{\omega}_i + 1) \qquad i = 1, 2, 3 \tag{11}$$

This expresses the low-frequency character of the disturbances. Parameter $\tilde{\omega}_i$ models the frequency beyond which the disturbance is small, whereas υ_i models the typical magnitude of the disturbance. The values of υ_i and $\tilde{\omega}_i$ are based on experience and intuition. Some parameters are chosen as a function of the nominal operating point (x_{1_0}, x_{2_0}). The disturbance $\bar{w}_1$ is assumed to be caused by aircleaner effects and is typically 10 Hz or smaller: $\tilde{\omega}_1 = 2\pi\, 10/\omega_H$. In addition, υ_1 is fixed at a fraction 0.01 of the dimensionless ambient pressure: $\upsilon_1 = 0.01[p_a/(\omega_c^2 r_T^2 \rho_a/2)]$. For $\bar{w}_2$, $\tilde{\omega}_2$ is also chosen $2\pi\ 10/\omega_H$, while it is assumed that the magnitude of $\bar{w}_2$ is a fraction 0.10 of the nominal mass flow: $\upsilon_2 = 0.10x_{1_0}$. For $\bar{w}_3$, $\tilde{\omega}_3$ is assumed to be related to the rotor speed ω_c: $\tilde{\omega}_3 = \omega_c N_b/\omega_H$. Moreover, υ_3 is fixed at a fraction 0.05 of the nominal pressure rise: $\upsilon_3 = 0.05x_{2_0}$.

The exogenous variables $\bar{w}$ also include sensor noise (y noise) $\bar{w}_4, \ldots, \bar{w}_7$. Experimental results for the laboratory setup with a mass flow and pressure sensor are used to estimate the magnitude of the noise. More specifically, rms values for mass flow measurements ($\theta_1 = 1.10 \times 10^{-3}$ kg/s) and pressure measurements ($\theta_2 = 220$ Pa) are used to characterize the magnitude of the y noise. Assuming white noise, the shaping filters are taken constant:

$$V_4 = \theta_1/\omega_c r_T \rho_a A_c \tag{12}$$

$$V_5 = V_6 = V_7 = \theta_2\big/\left(\omega_c^2 r_T^2 \rho_a/2\right) \tag{13}$$

The denominators make the mass flow and pressures dimensionless, as in Eq. (2).

The weighting filters for the compressor mass flow $\bar{z}_1 = x_1$ and the plenum pressure rise $\bar{z}_2 = x_2$ (x weights) are chosen constant:

$$W_1 = \rho_1\big/x_{1_0} \tag{14}$$

$$W_2 = \rho_2\big/x_{2_0} \tag{15}$$

The denominators scale the relative magnitudes of the controlled variables, which serves a better comparison of $\bar{z}_1$, $\bar{z}_2$, and the other controlled variables. These scalings actually apply to the deviations of the linear versions of x_1 and x_2 from zero, but these deviations could be expressed as a fraction of the nominal values x_{1_0} and x_{2_0} of the states of $\bar{G}_{\text{nl}}$. Parameters ρ_1 and ρ_2 are used to obtain satisfactory closed-loop responses; see Sec. IV.B.

The controlled variables also include actuator weights (u weights) $[\bar{z}_3\ \ \bar{z}_4\ \ \bar{z}_5]^T = u$. For the close-coupled valve and bleed valve, respectively,

$$W_3(s) = \left(\frac{\rho_3}{u_{1_0} - 1}\right)\frac{s/\tilde{\omega}_4 + 1}{s/\tilde{\omega}_0 + 1} \tag{16}$$

$$W_4(s) = \left[\frac{\rho_4}{\min\left(u_{2_0}, 1 - u_{2_0}\right)}\right]\frac{s/\tilde{\omega}_5 + 1}{s/\tilde{\omega}_0 + 1} \tag{17}$$

High-frequency inputs cannot be realized because the bandwidths of the valves are limited. A value of $\tilde{\omega}_0 = 10^6$ is large enough for W_3 and W_4 to have the desired high-pass character in the frequency range of interest up till $\tilde{\omega} = 10^5$. It is assumed that both valves have a bandwidth of 100 Hz: $\tilde{\omega}_4 = \tilde{\omega}_5 = 2\pi\, 100/\omega_H$. For the nonlinear model $u_1 \in [1, \infty)$ and $u_2 \in [0, 1]$. So, for the linear model $u_1 \in [1 - u_{1_0}, \infty)$ and $u_2 \in [-u_{2_0}, 1 - u_{2_0}]$. A stronger (symmetric) restriction is used, requiring the same absolute-valued bounds on positive and negative inputs: $\pm|1 - u_{1_0}|$ for u_1 and $\pm\min(|-u_{2_0}|, |1 - u_{2_0}|)$ for u_2. The reciprocals of these bounds are used in W_3 and W_4 to account for valve saturation. For the movable wall

$$W_5(s) = \left(\frac{\rho_{5_1}}{u_{3_{\max,1}}} + \frac{\rho_{5_2}}{u_{3_{\max,2}}}\frac{1}{s + 10^{-6}}\right)\frac{s/\tilde{\omega}_6 + 1}{s/\tilde{\omega}_0 + 1} \tag{18}$$

This combines limiting the movable wall's velocity u_3 and its displacement $\int u_3(\tilde{t})\, d\tilde{t}$, which are both bounded by the physical construction, into a single controlled variable. If the movable wall is constructed as a moving plate, it is assumed that $\tilde{\omega}_6 = 2\pi\, 50/\omega_H$ is suitable to avoid that u_3 contains too high frequencies. It is also assumed that the maximum velocity is 1.0 m/s. With $u_{3_0} = 0$ the maximum dimensionless velocity in the linear model is $u_{3_{\max,1}} = 1.0/(V_p\omega_H/A_p)$. The "almost integrator" $1/(s + 10^{-6})$ in W_5 accounts for the displacement limitation. The maximum displacement is assumed to be 0.05 m, giving $u_{3_{\max,2}} = 0.05/(V_p/A_p)$ as the maximum dimensionless displacement. The reciprocals of $u_{3_{\max,1}}$ and $u_{3_{\max,2}}$ in Eq. (18) account for actuator saturation. In the next section ρ_3, ρ_4, ρ_{5_1}, and ρ_{5_2} are determined.

B. Design Parameters

The NP control goal is stabilization in the face of disturbances, noise, and actuator limitations. The latter involves bounds on the $\mathcal{L}_\infty$ signal norm (i.e., the supremum of the absolute value over time) of u and of $\int u_3(\tilde{t})\, d\tilde{t}$. Transforming such requirements into the $\mathcal{H}_\infty$ system norm setting is not straightforward because bounding the amplitudes of $\bar{z}$ is not directly linked to the frequency domain and the $\mathcal{H}_\infty$ norm of a TFM. As an approximate solution, $\mathcal{H}_\infty$ optimizations and simulations are performed iteratively to determine the ρ parameters in the x weights and u weights. This is done for the full IO set, and $\omega_{c_3} = (2\pi/60)80{,}000$ rad/s. The simulations are performed for both the linear and nonlinear closed-loop systems. The main focus is on $x_{1_0} = F$: Fig. 5 shows that the eigenvalue with the largest positive real part (λ_1) occurs for $x_{1_0} = F$, and therefore achieving NP for $x_{1_0} = F$ is probably more difficult than for other $x_{1_0} \in [F, 3F]$. It is required and verified that the ρ parameters determined for $x_{1_0} = F$ also give acceptable responses for controllers designed with the same ρ parameters, but for other x_{1_0}.

The closed-loop behavior is evaluated as follows. Starting from a specified nominal operating point (x_{1_0}, x_{2_0}), the following three disturbances are applied:

$$\bar{w}_1(\tilde{t}) = \pm 0.5\upsilon_1 \exp\{-\tilde{\omega}_1\tilde{t}\} \qquad \tilde{t} \in [0, \tilde{t}_e] \tag{19}$$

$$\bar{w}_2(\tilde{t}) = \begin{cases} 0 & \tilde{t} \in [0, \Delta\tilde{t}) \\ \pm\upsilon_2 \exp\{-\tilde{\omega}_2(\tilde{t} - \Delta\tilde{t})\} & \tilde{t} \in [\Delta\tilde{t}, \tilde{t}_e] \end{cases} \tag{20}$$

$$\bar{w}_3(\tilde{t}) = \begin{cases} 0 & \tilde{t} \in [0, 2\Delta\tilde{t}) \\ \pm\upsilon_3 \exp\{-\tilde{\omega}_3(\tilde{t} - 2\Delta\tilde{t})\} & \tilde{t} \in [2\Delta\tilde{t}, \tilde{t}_e] \end{cases} \tag{21}$$

with $\tilde{t}_e$ the dimensionless end time of the simulation and $\Delta\tilde{t} = 2$ the dimensionless time between the disturbances. The latter is chosen such that $\bar{w}_1$ ($\bar{w}_2$) is negligible once $\bar{w}_2$ ($\bar{w}_3$) occurs. Recall that $\bar{w}_3$ is related to the rotor speed and is much faster than $\bar{w}_1$ and $\bar{w}_2$: $\tilde{\omega}_1 = \tilde{\omega}_2 = 4.11$, while, for ω_{c_3}, $\tilde{\omega}_3 = 3.29 \times 10^3$. In Eqs. (19–21) $\pm$ indicates the direction of the disturbances: either the case with $\bar{w}_{1,2,3}$ all having positive sign or the case with $\bar{w}_{1,2,3}$ all having negative sign is simulated. Note that $\bar{w}_{1,2,3}$ belong to the class described by $V_{1,2,3}$, but they may not be representative for the disturbances occurring in practice. Sensor noise and input saturation are not simulated.

The following iterative strategy is used to find suitable ρ parameters. To start with, the ρ parameters are assigned an initial value. For $x_{1_0} = F$ an $\mathcal{H}_\infty$ optimization is then performed, and the linear closed-loop system is simulated. Based on the maximum absolute values of u and $\int_0^{\tilde{t}_e} u_3(\tilde{t})\, d\tilde{t}$ the values of ρ_3, ρ_4, ρ_{5_1}, and ρ_{5_2} are adjusted, while ρ_1 and ρ_2 are kept the same. Even with $\rho_{5_2} = 0$, the displacement of the movable wall can be kept within its limits, and so $\rho_{5_2} = 0$ is maintained. However, setting $\rho_1 = \rho_2 = 0$ in the x weights can lead to unacceptable behavior of the nonlinear closed-loop system. For disturbances [Eqs. (19–21)] in negative direction, x may not return to (x_{1_0}, x_{2_0}), but end up in a different equilibrium of the nonlinear closed-loop system (u nonzero, but relatively small). Moreover, the inputs can exceed their limits. This can be circumvented by using nonzero x weights: $\rho_1 = \rho_2 = 0.1$. The values $\rho_3 = 4.48 \times 10^{-2}$, $\rho_4 = 2.59 \times 10^{-3}$, and $\rho_{5_1} = 7.00 \times 10^{-2}$ are then determined, yielding $\|M\|_\infty = 0.90$.

Some simulation results are depicted in Fig. 6. The left plot in Fig. 6 shows the limit-cycle behavior of the uncontrolled nonlinear system $\tilde{G}_{\text{nl}}$. The right plot shows the response of the controlled nonlinear system. Simulations for other $x_{1_0} \in [F, 3F]$ showed that the nonlinear systems closed by the controllers obtained for the same ρ parameters are stable and that x returns to the nominal operating point.

The ρ parameters determined for the full IO set will also be used for the other IO sets, both for the $\mathcal{H}_\infty$ optimizations in Sec. V and for the IO selection in Sec. VI. The results for the other IO sets may not be optimal then: iterative $\mathcal{H}_\infty$ optimizations and simulations for each IO set individually can give other ρ parameters and better responses. The reason to, nevertheless, use the same ρ parameters is twofold. First, it would be burdensome to perform the iteration for each candidate IO set. Second, to compare the IO sets based on the best achievable $\mathcal{H}_\infty$ norms (not on the best achievable responses) the design filters must be the same. They must thus be representative for all IO sets, which is only guaranteed for control problems that exactly fit into the $\mathcal{H}_\infty$-norm setting because V and W are then straightforwardly and unambiguously derived from specifications in the frequency domain. This is not the case here, and the control objectives are only approximately quantified.

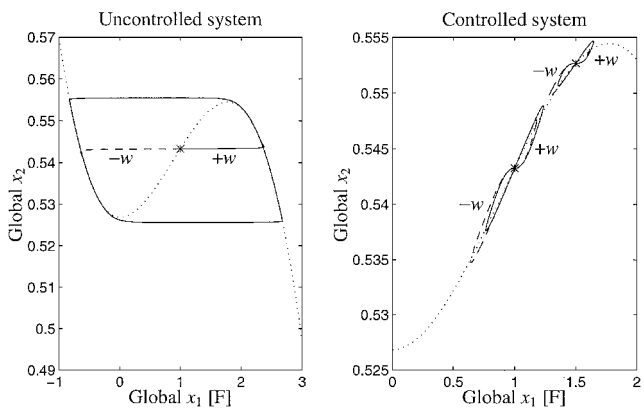

Fig. 6 Responses to disturbances $\bar{w}_1, \bar{w}_2, \bar{w}_3$ in two directions (indicated with $+w$ and $-w$) for speed ω_{c_3}. The nominal operating points are marked by $*$ and the equivalent compressor characteristic $\Psi_c(x_1) - (x_1|x_1|/c_1)u_{1_0}$ by $(\cdots)$. Left: open-loop response (counterclockwise). Right: closed-loop response: linear (——) and nonlinear system (– – –).

V. $\mathcal{H}_\infty$ Optimization for Typical IO Sets

To investigate the best achievable NP levels, $\mathcal{H}_\infty$ optimizations are performed. The design filters V and W from Sec. IV are used. Section V.A is devoted to the full IO set, whereas Sec. V.B compares some typical IO sets.

A. Influence of Operating Conditions

For the full IO set Fig. 7 shows the optimal values $\|M\|_\infty$ for speeds $\omega_{c_1}, \ldots, \omega_{c_5}$ and 21 nominal mass flows x_{1_0} evenly spaced in $[F, 3F]$. These values decrease for increasing x_{1_0}. Achieving NP is thus easier for larger mass flows. For ω_{c_3} this is made plausible via the pole location of $\tilde{G}$ (see Fig. 5). The two poles are real for all $x_{1_0} \in [F, 3F]$, except in a range (narrower for higher speeds) around $x_{1_0} = \alpha_{\text{cc}} F$. The poles are either both stable or both unstable. Starting from $x_{1_0} = F$, for increasing x_{1_0} the largest unstable pole λ_1 shifts toward the imaginary axis and then into the left half-plane. For static output feedback control in Ref. 6 it is also concluded that stabilization under bandwidth and gain limitations becomes easier if the slope of Ψ_c decreases, e.g., if x_{1_0} increases from F to $\alpha_{\text{cc}} F$. $\|M\|_\infty$ increases for increasing speeds, at least for small mass flows where the linearization is unstable. Achieving NP is thus more difficult for higher speeds, at least for the full IO set and in the unstable mass flow range. More generally, it was observed that in this range achieving NP is more difficult for a larger value of B in Eq. (5), e.g., as a result of a larger ω_c. This is in line with the observation in Ref. 6 that, for static output-feedback, stabilization under bandwidth and gain limitations is more difficult for larger B.

B. Comparison of Typical IO Sets

By considering IO sets with all four sensors and one actuator on the one hand and IO sets with all three actuators and one sensor on the other, insight can be obtained into the importance of each candidate actuator and sensor. Therefore, for the nine typical IO sets in Table 2 the optimal $\|M\|_\infty$ values are computed and compared in Figs. 8 and 9. All results are for $\omega_{c_3} = (2\pi/60)80{,}000$ rad/s and y noise, u weights, and x weights included. The stability of the open-loop system G (the empty IO set) and $\|G\|_\infty$ indicate whether control is needed or not. The $\mathcal{H}_\infty$ norm is only defined for stable TFMs, and so $\|G\|_\infty$ is only computed for the stable mass flow range, with and without close-coupled valve. Comparing $\|M\|_\infty$ with $\|G\|_\infty$ in the large mass flow range (say $x_{1_0} \in [2.4F, 3F]$), it appears that control does not improve NP: the open-loop system is already stable, and the controller provides only small actions to keep x_1 and x_2 small because limiting u is the dominant control objective. Simulations with

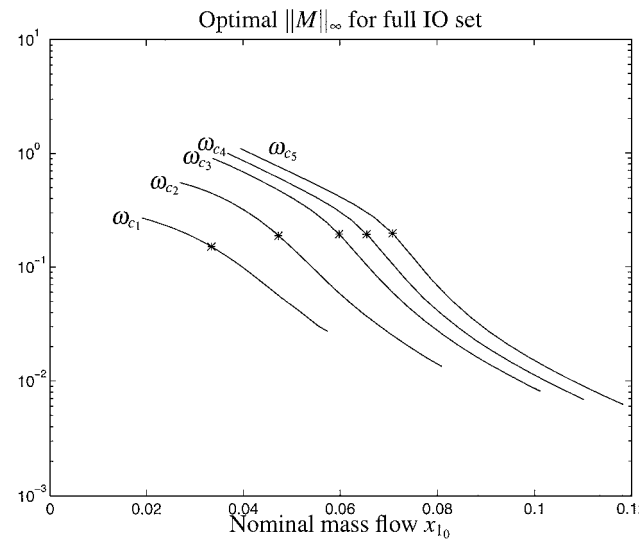

Fig. 7 $\|M\|_\infty$ from $\mathcal{H}_\infty$ optimizations for the full IO set and distinct speeds; $*$ indicates $x_{1_0} = \alpha_{\text{cc}} F$ where $\tilde{G}$ including the close-coupled valve goes from unstable to stable.

Table 2 Nine typical IO sets

IO set	Inputs	Outputs	Typical feature
1	$u_1u_2u_3$	$y_1y_2y_3y_4$	Full IO set
2	u_1	$y_1y_2y_3y_4$	Close-coupled valve
3	u_2	$y_1y_2y_3y_4$	Bleed valve
4	u_3	$y_1y_2y_3y_4$	Movable wall
5	$u_1u_2u_3$	y_1	Compressor mass flow
6	$u_1u_2u_3$	y_2	Plenum pressure rise
7	$u_1u_2u_3$	y_3	Total compressor face pressure
8	$u_1u_2u_3$	y_4	Static compressor face pressure
9	——	——	Empty IO set

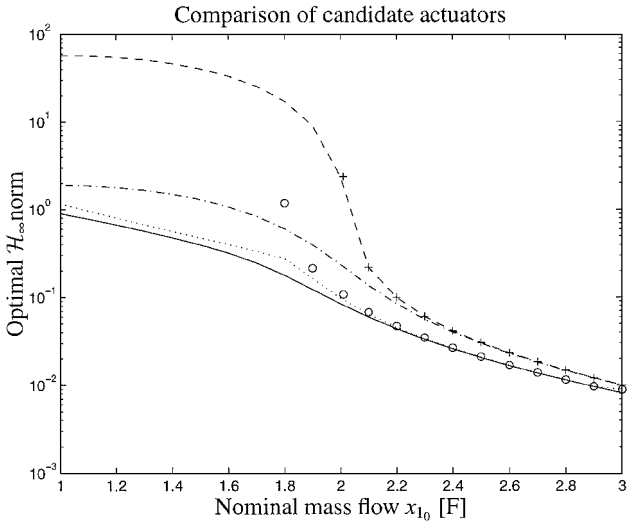

Fig. 8 Closed-loop norms $\|M\|_\infty$ from $\mathcal{H}_\infty$ optimizations for IO sets 1–4 in Table 2 (speed ω_{c_3}): full IO set 1 (——), IO set 2 with u_1 (· · · ·), IO set 3 with u_2 (– – –), IO set 4 with u_3 (–·–). Open-loop norms $\|G\|_\infty$ for the empty IO set 9 excluding the close-coupled valve (+) and including the close-coupled valve (o).

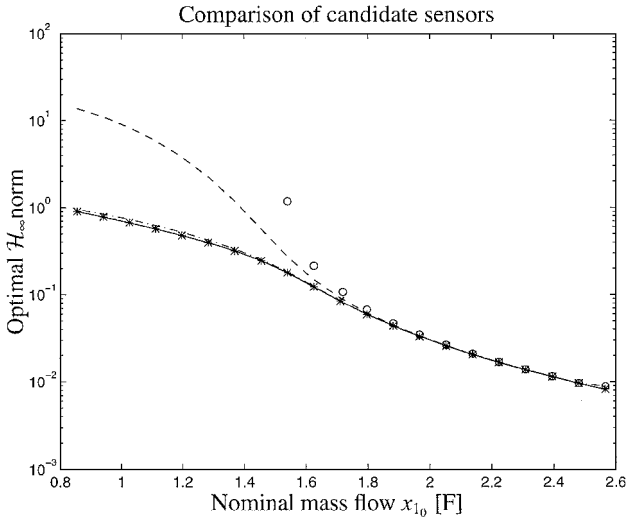

Fig. 9 Closed-loop norms $\|M\|_\infty$ from $\mathcal{H}_\infty$ optimizations for IO sets 1 and 5–8 in Table 2 (speed ω_{c_3}): full IO set 1 (——), IO set 5 with y_1 (· · · ·), IO set 6 with y_2 (– – –), IO set 7 with y_3 (–·–), IO set 8 with y_4 (∗). Open-loop norms $\|G\|_\infty$ for the empty IO set including the close-coupled valve (o).

disturbances Eqs. (19–21) show that the excursion from (x_{1_0}, x_{2_0}) is very small for both the uncontrolled and controlled system.

The actuator preference is studied via the optimal $\|M\|_\infty$ with IO sets 2–4 (see Fig. 8). The close-coupled valve u_1 is the best actuator, which is also found in Ref. 6. There it is stated that actuators close to the compressor are the most effective (an air injector in the compressor duct would also be promising). This is made plausible by studying the two eigenvalues and eigenvectors of $\bar{G}$. For

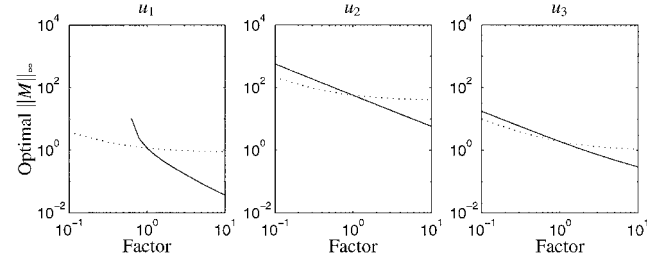

Fig. 10 Optimal $\|M\|_\infty$ for IO sets 2–4 and speed ω_{c_3} when the actuator bandwidths and maximum input magnitudes are varied by "Factor." Left: influence of u_{1_0} (——) and $\tilde{\omega}_4$ (· · · ·). Middle: influence of u_{2_0} (——) and $\tilde{\omega}_5$ (· · · ·). Right: influence of $u_{3_{\max,1}}$ (——) and $\tilde{\omega}_6$ (· · · ·).

small mass flows and speed ω_{c_3} the eigenvector corresponding to the largest unstable real pole λ_1 (see Fig. 5) almost entirely points into the direction of x_1, whereas for the eigenvector corresponding to λ_2 the contributions into direction x_1 and x_2 are about the same. For stabilization actuators directly acting upon the fast "compressor dynamics" [u_1, see Eq. (9)] are thus preferred to those directly acting upon the much slower "plenum dynamics" (u_2 and u_3). Section VI will show that other speeds can lead to different conclusions. The movable wall u_3 is the second best actuator, and the bleed valve u_2 is worst. This is caused by the large plenum volume V_p and small allowable magnitude of u_2. For a smaller V_p, $\|M\|_\infty$ with u_2 and u_3 decreases, whereas $\|M\|_\infty$ with u_1 remains almost unaffected.

The influence of the u weights on the achievable NP level is studied for IO sets 2–4. These weights account for the limited actuator bandwidths (via $\tilde{\omega}_4$, $\tilde{\omega}_5$, and $\tilde{\omega}_6$) and the maximum input magnitudes (via u_{1_0}, u_{2_0}, and $u_{3_{\max,1}}$). The movable wall's maximum displacement $u_{3_{\max,2}}$ is not considered, and the weight is set to zero: $\rho_{5_2} = 0$. The original design parameters are multiplied by a factor logarithmically spaced between 0.1 and 10. For the close-coupled valve this factor must be larger than $\frac{1}{1.72} = 0.58$ because the valve must be between fully open ($u_{1_0} = 1$) and fully closed ($u_{1_0} = \infty$). Only one parameter at a time is varied, and the optimal $\|M\|_\infty$ values are computed (all for $x_{1_0} = F$ and ω_{c_3}). In line with physical insight, Fig. 10 shows that $\|M\|_\infty$ decreases for increasing bandwidths and input magnitudes. Variation of the magnitude has a larger effect than variation of the bandwidth. In all cases the bleed valve u_2 is worst. The effect of actuator bandwidth was also studied in Ref. 6, leading to the conclusion that it strongly affects the possibilities for surge control by static output feedback. Clearly, the achievable NP level (and hence the IO selection results) can be strongly affected by the design parameters. On the one hand, the specifications must thus be accurately represented by the design filters to avoid erroneous results. On the other hand, if particular specifications are not final or fixed they could be modified until the desired $\mathcal{H}_\infty$ norm is achieved, while keeping the other specifications fixed. In this way the engineer could decide on properties like actuator bandwidth and sensor noise levels by manipulating the appropriate parameters in V and W.

The sensor preference is studied via the optimal $\|M\|_\infty$ with IO sets 5–8 (see Fig. 9). The mass flow sensor y_1 and the static compressor face pressure sensor y_4 are the best. The total compressor face pressure sensor y_3 is only slightly worse in the small mass flow range, whereas the plenum pressure rise sensor y_2 is clearly the worst. In Ref. 6 it was also found that y_1, y_3, and y_4 are better than y_2. There it is stated that sensors in the compressor duct (especially y_1) are the most promising, but that conclusion is based on static output feedback without y noise. For the dynamic output feedback considered here, it appears (no results depicted) that the optimal $\mathcal{H}_\infty$ norms with IO sets 5–8 become the same and equal to $\|M\|_\infty$ for the full output set if the y noise is reduced. This is explained as follows. For a control problem with no open-loop direct feedthrough from w to z, as for the problem at hand, full information feedback (see the third IO selection condition) becomes equivalent to state feedback (Ref. 11, Sec. 17.8). With an uncertainty-free model and observability with a single sensor (Ref. 8, Sec. 3.4), the observer-based $\mathcal{H}_\infty$ controller (Ref. 11, Sec. 16.8) employs perfectly reconstructed

states if there is no y noise. In this case adding sensors or using other ones does not improve the achievable NP level.

VI. IO Selection Results

In Sec. V.B, a subset of all candidate IO sets was subject to optimal controller design ($\min_K \|M\|_\infty$). In this section the $\mathcal{H}_\infty$ controller existence conditions are used to identify which IO sets among all candidates are viable, i.e., for which IO sets there exists a stabilizing controller achieving $\|M_\infty\| < \gamma$. This is done according to the IO selection procedure discussed in Sec. II. The design filters V and W, as determined in Sec. IV, are fixed for all IO sets. For the three candidate inputs and four candidate outputs there are seven candidate input sets, 15 candidate output sets, and (maximally) 106 candidate IO sets, including the empty one. The effect of different speeds and different NP level requirements γ is investigated, as well as the influence of skipping y noise, u weights, and x weights. The open-loop system is stable for $x_{1_0} \in (\alpha F, 3F]$. Figures 8 and 9 show that $\|G\|_\infty$ is relatively small there. Because the unstable mass flow range $[F, \alpha F]$ is more difficult to control (the empty IO set is always nonviable there), IO selection is only performed for this range. A grid of 11 evenly spaced points $x_{1_0} \in [F, 2F]$ is used, starting with $x_{1_0} = F$ and working toward $x_{1_0} = 2F$. Table 3 summarizes the results.

To start with, the focus is on rotor speed ω_{c_3} and $\gamma = 2$ that is more than twice the optimal $\|M\|_\infty = 0.90$ for the full IO set at $x_{1_0} = F$. IO selection is first performed without y noise, u weights, and x weights. Achieving NP then reduces to achieving nominal stability. All 105 nonempty IO sets are accepted because G is always stabilizable and detectable for a single input and output, respectively. All nonempty IO sets are still viable if y noise is added. In case of y noise and u weights, but no x weights, six candidates are accepted in the input selection step: the single bleed valve u_2 is rejected. In the output selection step 14 candidates are accepted: the single plenum pressure sensor y_2 is rejected. It was already observed from Figs. 8 and 9 that u_2 and y_2 are the least promising input and output. From the remaining 84 nonempty IO sets, two are eliminated in the third combined input/output selection step: u_1u_2/y_3 and u_1/y_3. This might not be expected because Fig. 8 suggests that the accepted IO set u_3/y_3 is worse than the rejected IO set u_1/y_3. The opposite is true, and failure of the last IO selection condition indicates that it is the combination of the input sets u_1u_2, u_1 and the output set y_3, which does not work well. If x weights are also included, the same 24 IO sets are rejected. Figures 8 and 9 show that for the typical IO sets the largest optimal $\mathcal{H}_\infty$ norms occur at $x_{1_0} = F$, where $\bar{G}$ has the largest unstable pole. For other $x_{1_0} \in [F, 2F]$ no additional IO sets are eliminated. This holds throughout this section, and so traversing the operating grid for x_{1_0} is not necessary for this particular problem. The reason is that the slope of the compressor characteristic in the range $[F, \ldots, 3F]$ is maximal for $x_{1_0} = F$. In the remainder y noise, u weights, and x weights are always included.

The focus is now on the same speed $\omega_{c_3} = (2\pi/60)80{,}000$ rad/s, but on a tightened NP level requirement $\gamma = 1$. In the input selection step only the full input set and u_1u_3, using the close-coupled valve and the movable wall, are accepted. In the output selection step all candidates but y_2 are accepted. The remaining 28 nonempty candidate IO sets are all accepted in the combined input/output selection step.

Table 3 Overview of IO selection results

Case	γ	Speed	y noise	u weights	x weights	Viable I sets	Viable O sets	Viable IO sets
1	2	ω_{c_3}	−[a]	−	−	7	15	105
2	2	ω_{c_3}	+[b]	−	−	7	15	105
3	2	ω_{c_3}	+	+	−	6	14	82
4	2	ω_{c_3}	+	+	+	6	14	82
5	1	ω_{c_3}	+	+	+	2	14	28
6	2	ω_{c_1}	+	+	+	4	14	56
7	2	ω_{c_2}	+	+	+	6	14	80
8	2	ω_{c_4}	+	+	+	4	14	54
9	2	ω_{c_5}	+	+	+	4	14	54
10	2	$\omega_{c_1}, \ldots, \omega_{c_5}$	+	+	+	2	14	28
11	3	$\omega_{c_1}, \ldots, \omega_{c_5}$	+	+	+	4	14	49

[a] − = excluded. [b] + = included.

Consider again $\gamma = 2$ and ω_{c_3}, for which 82 IO sets are viable. IO selection is now performed for $\gamma = 2$ and the other four speeds. For $\omega_{c_1} = (2\pi/60)40{,}000$ rad/s, 49 nonempty IO sets are eliminated: $u_1u_2/y_1y_2y_3y_4$ and its 44 subsets, and four IO sets using only y_2. For $\omega_{c_2} = (2\pi/60)60{,}000$ rad/s, 25 nonempty IO sets are eliminated: the 15 IO sets using only u_2, six IO sets based on the single y_2, the three IO sets u_1/y_3y_4, u_1/y_3, u_1/y_4 based on u_1 and compressor face pressure measurements, and finally u_1u_2/y_3. So, for ω_{c_1} and ω_{c_2} more IO sets are eliminated than for ω_{c_3}. This contradicts the conclusion for the full IO set in Sec. V.A that control is easier for lower speeds (for smaller B). $\mathcal{H}_\infty$ optimizations with the full output set show that the close-coupled valve u_1 does not work as well for ω_{c_1} as for ω_{c_3}, whereas the bleed valve u_2 and the movable wall u_3 perform better; u_3 is even better than u_1. For lower speeds the unstable compressor dynamics becomes slower (easier to stabilize), whereas the unstable plenum dynamics becomes faster (more difficult to stabilize). Using u_3, which directly acts upon the plenum dynamics, becomes more effective than using u_1, which acts more directly on the compressor dynamics. For both $\omega_{c_4} = (2\pi/60)90{,}000$ rad/s and $\omega_{c_5} = (2\pi/60)100{,}000$ rad/s, 51 nonempty IO sets are eliminated: $u_2u_3/y_1y_2y_3y_4$ and its 44 subsets, $u_1u_2u_3/y_2$ and three subsets, u_1u_2/y_3, and u_1/y_3. So, for ω_{c_4} and ω_{c_5} more IO sets are eliminated than for ω_{c_3}.

To examine which of the IO sets are accepted for $\gamma = 2$ and all five speeds $\omega_{c_1}, \ldots, \omega_{c_5}$, in each of the three steps of IO selection the five speeds are investigated in succession: starting with ω_{c_1}, accepted candidates are checked for speed ω_{c_2}, and so on. The 28 accepted IO sets all employ both the close-couple valve u_1 and the movable wall u_3 and at least one of the sensors y_1, y_3, or y_4. These are the same IO sets as accepted for $\gamma = 1$ and ω_{c_3}. IO sets u_1u_3/y_1, u_1u_3/y_3, and u_1u_3/y_4 are the smallest accepted candidates. The IO sets accepted for $\gamma = 2$ and all five speeds use at least two actuators. To find out which IO sets with one actuator are most promising, IO selection for all speeds is performed for a relaxed NP level $\gamma = 3$. The only viable 1×1 IO set is u_1/y_1.

VII. Conclusions

For active surge control IO selection was performed for a nonlinear compression system model with a Garrett GT45 turbocharger. The close-coupled valve u_1 and movable wall u_3 combined with the compressor mass flow sensor y_1 yields the best, smallest (2×1) IO set. Pressure sensors y_3 and y_4 can be substituted for a small decrease in performance, being more cost effective. This conclusion can be tied to the particular plant and performance specifications. Among the 1×1 IO sets, u_1/y_1 is the most promising, as also concluded in Ref. 6. For most IO sets good performance is more difficult to achieve for higher rotor speeds or, more generally, for a larger B parameter. This does not hold for IO sets based on the close-coupled valve u_1 because of the plenum dynamics (which is not directly affected by u_1) becoming relatively more difficult to control for lower speeds. This conclusion can be tied to the choice of working-point-dependent weights.

Though the IO selection method was originally developed for linear systems, it appeared to be useful for the nonlinear compression system as well. Based on linearizations for a grid of nominal operating points (equilibria), the local viability of IO sets is assessed. Their global viability remains undecided. To assess this, additional studies (simulations, computing the attraction regions) must be performed after IO selection.

To quantify the control objectives, the IO selection method employs design filters. These must be chosen properly to obtain useful results, which can be problematic if the performance specifications are not exactly known or not fixed. For the compression system little information on the disturbances is available, and there is some freedom in the choice of the actuator bandwidths and maximum input magnitudes. It was shown that the achievable performance level is sensitive to the actuator specifications. Varying the design parameters that represent actuator and sensor limitations can be useful to obtain insight into the desired instrumentation. The control

objectives should also match the $\mathcal{H}_\infty$-norm setting. For the compression system this does not hold for the inputs that must stay within bounds. To find suitable weights, an iterative procedure of controller design, simulation, and design filter adaptation for the full IO set was used. Though the transformation into the $\mathcal{H}_\infty$-norm setting was only approximate, the IO selection results fit in with the problem's physics.

References

[1]De Jager, B., "Rotating Stall and Surge Control: A Survey," *Proceedings of the 34th IEEE Conference on Decision and Control*, Vol. 2, Inst. of Electrical and Electronics Engineers, Piscataway, NJ, 1995, pp. 1857–1862.

[2]Gu, G., Sparks, A., and Banda, S. S., "An Overview of Rotating Stall and Surge Control for Axial Flow Compressors," *IEEE Transactions on Control Systems Technology*, Vol. 7, No. 6, 1999, pp. 639–647.

[3]Willems, F., and De Jager, B., "Modeling and Control of Compressor Flow Instabilities," *IEEE Control Systems Magazine*, Vol. 19, No. 5, 1999, pp. 8–18.

[4]Van de Wal, M., and De Jager, B., "A Review of Methods for Input/Output Selection," *Automatica—J. IFAC*, Vol. 37, No. 4, 2001, pp. 487–510.

[5]Van de Wal, M., and De Jager, B., "Selection of Sensors and Actuators for an Active Suspension Control Problem," *Proceedings of the 5th IEEE Conference on Control Applications*, Inst. of Electrical and Electronics Engineers, Piscataway, NJ, 1996, pp. 55–60.

[6]Simon, J. S., Valavani, L., Epstein, A. H., and Greitzer, E. M., "Evaluation of Approaches to Active Compressor Surge Stabilization," *Journal of Turbomachinery*, Vol. 115, No. 1, 1993, pp. 57–67.

[7]Montazeri-Gh, M., Allerton, D. J., and Elder, R. L., "Actuator Placement for Active Surge Control in a Multi-Stage Compressor," *Proceedings of the International Gas Turbine and Aeroengine Congress and Exhibition*, American Society of Mechanical Engineers, New York, Paper 96-GT-241, 1996.

[8]Van de Wal, M., and Willems, F., "Selection of Actuators and Sensors for Compressor Control," Faculty of Mechanical Engineering, Eindhoven Univ. of Technology, Rept. WFW 96.155, The Netherlands, Nov. 1996.

[9]Van de Wal, M., "Selection of Inputs and Outputs for Control," Ph.D. Dissertation, Faculty of Mechanical Engineering, Eindhoven Univ. of Technology, The Netherlands, April 1998.

[10]Glover, K., and Doyle, J. C., "State-Space Formulae for All Stabilizing Controllers That Satisfy an $\mathcal{H}_\infty$-Norm Bound and Relations to Risk Sensitivity," *Systems and Control Letters*, Vol. 11, No. 2, 1988, pp. 167–172.

[11]Zhou, K., Doyle, J. C., and Glover, K., *Robust and Optimal Control*, Prentice–Hall, Upper Saddle River, NJ, 1996.

[12]Van der Schaft, A. J., *$\mathcal{L}_2$-Gain and Passivity Techniques in Nonlinear Control*, Lecture Notes in Control and Information Sciences, Vol. 218, Springer-Verlag, Heidelberg, 1996.

[13]Van Essen, H., "Design of a Laboratory Gas Turbine Installation," Faculty of Mechanical Engineering, Eindhoven Univ. of Technology, Rept. WOC-WET 95.012, The Netherlands, March 1995.

[14]Greitzer, E. M., "Surge and Rotating Stall in Axial Flow Compressors. Part I: Theoretical Compression System Model," *Journal of Engineering for Power*, Vol. 98, No. 2, 1974, pp. 190–198.

[15]Gravdahl, J. T., and Egeland, O., "Centrifugal Compressor Surge and Speed Control," *IEEE Transactions on Control Systems Technology*, Vol. 7, No. 5, 1999, pp. 567–579.

[16]Willems, F., "Modeling and Control of Compressor Flow Instabilities," Faculty of Mechanical Engineering, Eindhoven Univ. of Technology, Rept. WFW 96.151, The Netherlands, June 1997.

[17]Willems, F., Heemels, M., De Jager, B., and Stoorvogel, A., "Positive Feedback Stabilization of Surge in a Centrifugal Compressor," *Proceedings of the 38th IEEE Conference on Decision and Control*, Inst. for Electrical and Electronics Engineers, Piscataway, NJ, 1999, pp. 3259–3264.